AFRL-RX-WP-TP-2011-4221

ON THE ROOM-TEMPERATURE ANNEALING OF CRYOGENICALLY-ROLLED COPPER (Preprint)

S.L. Semiatin

Metals Branch
Metals, Ceramics & NDE Division

T. Konkova1 and A. Korznikov

Russian Academy of Science
Institute for Metals Superplasticity Problems

S. Mironov

Tohoku University
Graduate School of Engineering

JULY 2011

AIR FORCE RESEARCH LABORATORY
MATERIALS AND MANUFACTURING DIRECTORATE
WRIGHT-PATTERSON AIR FORCE BASE, OH 45433-7750
AIR FORCE MATERIEL COMMAND
UNITED STATES AIR FORCE

REPORT DOCUMENTATION PAGE

Form Approved
OMB No. 0704-0188

1. REPORT DATE *(DD-MM-YY)*	2. REPORT TYPE	3. DATES COVERED *(From - To)*
July 2011	Journal Article Preprint	01 July 2011 – 01 July 2011

4. TITLE AND SUBTITLE

ON THE ROOM-TEMPERATURE ANNEALING OF CRYOGENICALLY-ROLLED COPPER (Preprint)

5a. CONTRACT NUMBER
IN-HOUSE

5b. GRANT NUMBER

5c. PROGRAM ELEMENT NUMBER
62102F

6. AUTHOR(S)

S.L. Semiatin (Metals, Ceramics & NDE Division, Metals Branch (AFRL/RXLM))
T. Konkova1 and A. Korznikov (Russian Academy of Science, Institute for Metals Superplasticity Problems)
S. Mironov (Tohoku University, Graduate School of Engineering)

5d. PROJECT NUMBER
4347

5e. TASK NUMBER
20

5f. WORK UNIT NUMBER
LM106500

7. PERFORMING ORGANIZATION NAME(S) AND ADDRESS(ES)

Metals, Ceramics & NDE Division, Metals Branch (AFRL/RXLM)
Materials and Manufacturing Directorate, Air Force Research Laboratory
Wright-Patterson Air Force Base, OH 45433-7750
Air Force Materiel Command, United States Air Force

Russian Academy of Science
Institute for Metals Superplasticity Problems

Tohoku University
Graduate School of Engineering

8. PERFORMING ORGANIZATION REPORT NUMBER
AFRL-RX-WP-TP-2011-4221

9. SPONSORING/MONITORING AGENCY NAME(S) AND ADDRESS(ES)

Air Force Research Laboratory
Materials and Manufacturing Directorate
Wright-Patterson Air Force Base, OH 45433-7750
Air Force Materiel Command
United States Air Force

10. SPONSORING/MONITORING AGENCY ACRONYM(S)
AFRL/RXLM

11. SPONSORING/MONITORING AGENCY REPORT NUMBER(S)
AFRL-RX-WP-TP-2011-4221

12. DISTRIBUTION/AVAILABILITY STATEMENT
Approved for public release; distribution unlimited.

13. SUPPLEMENTARY NOTES
PAO case number 88ABW-2011-1490, cleared 16 March 2011. This work was funded in whole or in part by Department of the Air Force work unit LM106500. The U.S. Government has for itself and others acting on its behalf an unlimited, paid-up, nonexclusive, irrevocable worldwide license to use, modify, reproduce, release, perform, display, or disclose the work by or on behalf of the U. S. Government. Submitted to Acta Materialia. Document contains color.

14. ABSTRACT
The electron-backscatter-diffraction (EBSD) technique was applied to investigate room-temperature annealing processes in cryogenically-rolled copper during long-term (~1.5 years) storage at ambient temperature. Static recrystallization appeared to be nucleated as result of both grain-boundary bulging and recovery. A bimodal recrystallized grain-size distribution appeared to be a result of these two competing mechanisms.

15. SUBJECT TERMS
cryogenic deformation, electron backscatter diffraction, copper, recrystallization, microstructure, texture

16. SECURITY CLASSIFICATION OF:			17. LIMITATION OF ABSTRACT:	18. NUMBER OF PAGES	19a. NAME OF RESPONSIBLE PERSON (Monitor)
a. REPORT	b. ABSTRACT	c. THIS PAGE			Lee Semiatin
Unclassified	Unclassified	Unclassified	SAR	32	19b. TELEPHONE NUMBER *(Include Area Code)* N/A

Standard Form 298 (Rev. 8-98)
Prescribed by ANSI Std. Z39-18

On the room-temperature annealing of cryogenically-rolled copper

T. Konkova[1], S. Mironov[1,2], A. Korznikov[1], and S.L. Semiatin[3]

[1]Institute for Metals Superplasticity Problems, Russian Academy of Science, 39 Khalturin Str., Ufa, 450001, Russia
[2]Department of Materials Processing, Graduate School of Engineering, Tohoku University, 6-6-02 Aramaki-aza-Aoba, Sendai 980-8579, Japan
[3]Air Force Research Laboratory, Materials and Manufacturing Directorate, AFRL/RXLM, Wright-Patterson AFB, OH 45433-7817, USA

The electron-backscatter-diffraction (EBSD) technique was applied to investigate room-temperature annealing processes in cryogenically-rolled copper during long-term (~1.5 years) storage at ambient temperature. Static recrystallization appeared to be nucleated as result of both grain-boundary bulging and recovery. A bimodal recrystallized grain-size distribution appeared to be a result of these two competing mechanisms.

Keywords: Cryogenic deformation; Electron backscatter diffraction; Copper; Recrystallization; Microstructure; Texture

1. INTRODUCTION

There is currently a considerable interest in the potential use of cryogenic deformation for the production of nanocrystalline materials [e.g. 1-5]. It is believed that very low temperatures may greatly suppress dynamic recovery and stimulate mechanical twinning, thereby enhancing the grain-refinement effect. To date, the majority of the research in this field has focused on aluminum and copper alloys, most likely because of the superior ductility of these materials.

In previous work [5], the electron-backscattered-diffraction (EBSD) technique was employed to investigate microstructure evolution during cryogenic rolling of copper. It was found that the cryo-rolled material was unstable during long-term (~1.5 years) storage at room temperature after deformation; clear evidence of partial recrystallization was observed. The recrystallization was deduced to be discontinuous in nature and to have originated from strain-induced grain-boundary migration.

A review of the scientific literature reveals that the room-temperature recrystallization of cryo-deformed copper was described ~45 years ago [6], but many details of this unusual phenomenon are still unclear. Because the annealing process occurs at a very low homologous temperature (~$0.2T_m$), it is of interest, therefore, to establish possible similarities with more conventional, higher-temperature recrystallization phenomena. Such a modern investigation is facilitated by the application of EBSD with its very sophisticated microstructure-analysis capabilities. In this regard, several EBSD approaches have been recently applied for detection and quantification of the recrystallized phase in a partially-recrystallized material [e.g. 7-10]. The objective of the present work was

to apply these advanced EBSD techniques to gain further insight into the room-temperature annealing behavior of cryogenically-rolled copper.

2. MATERIAL AND EXPERIMENTAL PROCEDURES

The material used in the present work consisted of 99.9 wt. pct. pure copper supplied as a hot-rolled bar. The as-received material was preconditioned by severe plastic deformation and then cryogenically rolled to 50, 75, or 93 pct. overall thickness reductions (true strains of 0.7, 1.4 and 2.7). The total thickness reduction was achieved using multiple passes of ~10 pct. each. In order to provide cryogenic-deformation conditions, the rolling preform and work rolls were soaked in liquid nitrogen prior to each pass and held for 20 minutes. Immediately after the pass, the workpiece was re-inserted into liquid nitrogen. The total time for each pass (i.e., the exposure time of the specimen under ambient conditions) was only a few seconds. Heat transfer calculations revealed that the warming of the rolls and copper specimens prior to rolling due to free convection in air was small, resulting in temperature increases of the order of only ~1-4°C.

The microstructure of the cryogenically-rolled specimens was determined after storage at room temperature for ~1.5 years. To allow a better comparison with the data presented in literature, EBSD observations were made on the longitudinal plane containing the rolling and normal directions. (In this work, the typical flat-rolling convention was adopted with RD being the rolling direction, TD the long-transverse direction, and ND the normal direction of the sheet). Samples for EBSD were prepared by mechanical polishing followed by electro-polishing in a solution of 70% orthophosphoric acid in water at ambient temperature with an applied potential of 5 V. All microstructure and texture observations were made at the mid-thickness of the rolled specimens.

High-resolution EBSD analysis was conducted with a field-emission-gun scanning electron microscope (FEG-SEM) equipped with a TSL OIM^{TM} EBSD system. The EBSD scans consisted of ~350,000-500,000 pixels and were acquired with a scan step size of 50 or 250 nm. To minimize measurement errors, all grains comprising less than 3 pixels were automatically removed from the maps before data analysis. In addition, to eliminate spurious boundaries caused by orientation noise, a lower-limit boundary-misorientation cut-off of 2° was used. A 15° criterion was used to differentiate low-angle boundaries (LABs) and high-angle boundaries (HABs). The grain size in the recrystallized phase was quantified by measurement of grain area (ignoring annealing twin boundaries) and calculation of the equivalent grain diameter assuming each grain as a circle (i.e., the so-called grain reconstruction method [11]). For the deformed phase, the grain thickness was measured using the linear-intercept method.

3. EBSD DATA-ANALYSIS PROCEDURES

Room-temperature annealing of cryogenically rolled copper occurs relatively slowly. When the present microstructural observations were made (~1.5 years after deformation), recrystallization was not complete, and the material had a partially-recrystallized microstructure. Although several EBSD approaches for

partitioning of the recrystallized and partially-recrystallized phases [e.g. 7-10] have been proposed recently, the problem is not trivial. Thus, the applicability of the various methods for the present work is discussed in this section.

3.1. Image quality and confidence index

One of the first EBSD techniques to be applied to quantify retained work is based on the measurements of the sharpness of the Kikuchi-patterns (i.e., the so-called "image quality"), which is closely linked with the defect content in the area that is probed [7]. An example image-quality (IQ) map for the cryo-rolled material is shown in Fig. 1a; here, lighter and darker regions denote higher and lower IQ values. A number of grains with high IQ are evident; based on the specific morphology and high IQ value, these grains may presumably be associated with recrystallized material. A similar, contrast-based approach is often used in conventional etched-specimen metallography; an IQ map is usually similar to the corresponding optical (or SEM) image of a microstructure.

Crystal defects are known to weaken the Kikuchi bands, thus affecting the correctness of the automatic indexing of diffraction patterns during EBSD. This may also be used for detection of the recrystallized phase. In the software employed for present study, the degree of confidence that the indexing is correct is defined by the so-called confidence index [12]. The CI map of the same region as in Fig. 1a is shown in Fig. 1b; the CI value increases with increasingly lighter shades of gray. A comparison of Figs. 1a and 1b reveals that the IQ and CI maps are broadly similar to each other, thus supporting the assumption that bright grains belong to the recrystallized phase.

Unfortunately, both of these methods have significant drawbacks. The IQ and CI are known to decrease significantly near grain boundaries due to the overlapping of Kikuchi-patterns from neighboring grains. Thus, recrystallized grains may contain pixels with low IQ and CI. Moreover, although bright grains are clearly seen in IQ and CI maps, their borders are blurred. Thus, the selection of the proper IQ or CI tolerance separating the deformed and recrystallized phases is difficult and largely subjective. Furthermore, the IQ and CI may be influenced by crystal orientation and experimental setup.

3.2. Grain orientation spread (GOS)

Another EBSD approach is based on the idea that recrystallized grains should have a low orientation spread [8-10]. In this case, EBSD software systematically measures variations of crystallographic orientation within grains. Recrystallized grains are usually defined as those having an orientation spread below the EBSD angular resolution limit (typically ~2°). This tolerance value has a clear physical meaning, and, therefore, the orientation-spread method appears to be more objective than IQ or CI.

The GOS approach is influenced by the grain definition, however. In the present work, grains were defined as crystallites bordered by a continuous boundary having a misorientation greater than 15°; i.e., a HAB. The orientation spread within each grain was determined by calculating the average deviation between the orientation of each pixel in the grain and the average orientation for

that grain. This enabled short-range as well as long-range orientation deviations within grains to be taken into account.

A GOS EBSD map for the same region as in Figs. 1a and 1b is shown in Fig. 1c. The grains with an orientation spread lower or higher than 2° are indicated as white or grey, respectively. The GOS map was not identical to the IQ and CI maps, but some similarity was evident. The observed discrepancy was partially attributable to the degradation of the IQ and CI in near-grain-boundary regions, as discussed above. As a result, white grains in the GOS map (Fig. 1c) were typically larger than the corresponding ones in the IQ and CI maps. Generally, grains with low orientation spread had relatively high IQ and CI (Fig. 2).

It should be noted that the evaluation of the orientation spread within grains accounts only for geometrically necessary dislocations [e.g. 8], but provides no information on statistically-stored component of the dislocation structure which produces no significant orientation variations. However, the approximate match between the EBSD maps in Figs. 1a-c suggests that the low-orientation-spread grains are characterized by low dislocation density.

During the development of the analysis procedure, it was found that some high IQ or CI grains had a measured orientation spread greater than the experimental error of 2°; an example is circled in Figs. 1a-c. This observation may indicate that even recrystallized grains may include some degree of residual deformation which is not completely eliminated. This interesting effect has been previously noted for the early stages of recrystallization [13,14], but its source has still not been resolved definitively. Nevertheless, it appears that recrystallized and deformed grains may overlap partially in terms of orientation spread, and the microstructure may not always readily fit into traditional categories.

3.3. Subboundary analysis

The nature of subboundaries developed within grains may also convey useful information for partitioning deformed and recrystallized microstructures. Here, subboundaries were analyzed in the context of the orientation-spread approach. As an example, the grain-orientation-spread map (Fig. 1c) was superimposed with subboundaries as shown in Fig. 1d; LABs, HABs and $\Sigma 3$ twin boundaries are depicted with green, black, and red lines, respectively[1]. LABs were found almost solely in grains with high orientation spread. On the other hand, $\Sigma 3$ boundaries were preferentially located in low-orientation-spread grains. In face-centered cubic (FCC) metals of intermediate or low stacking fault energy (including copper), recrystallization is typically accompanied by the formation of annealing twins, and therefore the observed high twin fraction in the recrystallized phase here was as expected. Thus, the character of the spatial distribution of LABs and $\Sigma 3$ boundaries supports the conclusion that low-orientation-spread grains were indeed recrystallized.

Figure 1d also reveals that there were several grains without LABs (or annealing twins), with high IQ and CI, but also exhibiting an orientation spread

[1] For this and subsequent figures in color, the reader is referred to the on-line version of the paper.

greater than 2°; an example is circled in this figure. This finding supports the above idea that the defect structure may not be completely eliminated in some recrystallized grains.

Quantitative boundary misorientation data for the low- and the high-orientation-spread grains (Fig. 3) also revealed the efficacy of using the orientation-spread approach for delineation of the recrystallized phase. The misorientation distribution for the low-orientation-spread grains was dominated by twin boundaries creating a sharp peak near 60^{o} (Fig. 3a). The misorientation across the twin boundaries was typically very close to the ideal $\Sigma 3$ (Fig. 3b). This confirmed that the twins developed during annealing, for the precise twin-matrix orientation relation would have been destroyed during additional deformation following the formation of mechanical twins [15]. The high-orientation-spread grains also contained a small fraction of twin boundaries, but their misorientations exhibited significant deviations from the perfect $\Sigma 3$ relationship (Fig. 3b). Hence, these latter features may be remnants of mechanical twins developed during cryogenic deformation of copper [e.g. 2,3,5]. Moreover, the high-orientation-spread grains also included a small fraction of the annealing twins, as noted above.

The results in Fig. 3a also revealed the unexpected observation that the low-orientation-spread grains contained a non-negligible fraction of LABs typically having very low (~3°) misorientation (Fig. 3a). This effect has also been reported in literature [13,16] and is consistent with the above hypothesis regarding remnant substructure in some nominally-recrystallized grains.

3.4. Texture analysis

Recrystallization in FCC metals may give rise to very specific textures. Thus, preferential grain orientations may also be used for examination of the reliability of the orientation-spread approach for partitioning microstructure. Orientation distribution functions (ODFs) for the low- and the high-orientation-spread grains are given in Fig. 4. For comparison purposes, the ideal rolling and recrystallization texture components for FCC metals are summarized in Table 1. Fig. 4 indicates that the textures were distinctly different for the two groups of grains. For the high-orientation-spread grains, the texture was relatively strong (~13 times random), being dominated by the Brass {011}<211>, Goss {011}<100>, and S_3 {123}<634> rolling components (Fig. 4a, Table 1). For the low-orientation-spread grains, the texture was much weaker (~5 times random); it consisted of a mixture of S_3 {123}<634> rolling texture and Q {013}<231> and cube {001}<100> recrystallization components (Fig. 4b, Table 1). Therefore, texture analysis provides additional support for the use of the orientation-spread method to partition microstructure data.

3.5. Summary

For the present application, it has been concluded that the IQ approach may be useful for the qualitative evaluation of recrystallized material, but can be rather speculative for quantitative results. The orientation-spread method is more objective and yields generally reliable data. Thus, this latter technique was used as the principal tool for data analysis. It should be noted, however, that the

border between recrystallized and deformed material is sometimes blurred, and observed microstructures do not always fit readily into one of the two categories. To underscore such uncertainty, the terms “recrystallized” and “deformed” in quotation marks are used below.

4. RESULTS AND DISCUSSION

4.1. Microstructure morphology and grain size

The full range of microstructural features was delineated in EBSD grain-orientation-spread (GOS) maps obtained with scan step sizes of 0.25 μm (Fig. 5) or 0.05 μm (Fig. 6) from material cryogenically rolled to total thickness reductions of 50, 75, or 93 pct. In each map, “deformed” areas (with GOS $\geq 2°$) are gray, whereas “recrystallized” material (with GOS < 2°) is white. LABs, HABs, and Σ3 twin boundaries are depicted by green, black and red lines, respectively; for simplicity, LABs are omitted in Fig. 5. Grain-structure statistics for the “recrystallized” and “deformed” phases are given in Figs. 7 and 8, respectively.

4.1.1. “Recrystallized” phase

For the material rolled to a 50-pct. reduction, the “recrystallized” phase consisted of fine, low-aspect ratio grains (Figs. 5a and 6a). As shown in the lower-resolution map (Fig. 5a), the “recrystallized” grains were distributed relatively homogeneously with no clusters suggestive of the formation of localized deformation bands during the rolling operation. This observation indicates that the recrystallization nuclei developed uniformly throughout the material in a manner similar to recent findings for cryogenically-deformed aluminum [1] and copper [5]. In both of these earlier investigations, neither shear bands nor other coarse-scale plastic-flow heterogeneities, which may promote recrystallization, were noted. At the grain scale, on the other hand, the “recrystallized” grains tended to be concentrated preferentially along the boundaries or triple joints of the elongated “deformed” grains (Figs. 5a and 6a). Some of the “recrystallized” grains appeared to be twins (e.g., feature indicated by the arrow in Fig. 6a), thus suggesting that the formation of annealing twins may be associated with recrystallization. The EBSD results also showed that the “recrystallized” grains frequently contained LAB substructure; an example is circled in Fig. 6a. Such findings were discussed in Section 3.

The “recrystallized” grains in the material rolled to a 50-pct. reduction were typically less than 1 μm in diameter (Fig. 7a). This size was compared to the theoretical minimum value for a stable recrystallization nucleus as determined by the balance between its surface energy and the energy of stored dislocations eliminated by the formation of the nucleus [17]. The stored energy due to a dislocation density ρ is ~0.5 $\rho G b^2$, in which G denotes the shear modulus and b the Burgers vector of the dislocations. For copper, G ~ 4.2 x 10^{10} Nm^{-2} and b ~ 0.26 nm [17]); a dislocation density of 10^{15} m^{-2} thus corresponds to a stored energy of 1.4 x 10^6 Jm^{-3}. The energy stored per unit volume in a 3-D grain-boundary array is ~3γ/D, in which γ is the grain boundary energy per unit area (~0.5 Jm^{-2} for HABs in copper [17]) and D is the grain (nucleus) size. The criterion for nucleus growth, $D > 3\gamma / 0.5 G b^2 \rho$, leads to a critical nucleus size of

~1μm. Because the "recrystallized" grains developed in the material rolled to a 50-pct. reduction were typically smaller than 1 μm, they would be unstable and not able to grow.

In the material rolled to 75-pct. reduction, the "recrystallized" microstructure was still dominated by fine (<1 μm) low-aspect ratio grains (Figs. 5b, 6b and 7a). However, relatively coarse grains ~10 μm in size were also evident (Figs. 5b, 6b and 7a). These coarse grains were frequently not equiaxed but elongated in the RD (Fig. 5b). Moreover, they typically contained annealing twins (Fig. 5b and 6b). As discussed in Section 3, in FCC metals of intermediate or low stacking fault energy (including copper), the formation of annealing twins is associated mainly with grain-boundary migration during either primary recrystallization or grain growth. Thus, the extensive twinning in the coarse "recrystallized" grains provided clear evidence of the discontinuous nature of the recrystallization process. This conclusion is in agreement with previous work [5] in which the recrystallization was hypothesized to originate from strain-induced grain boundary migration.

After 93 pct. reduction, the fraction of the "recrystallized" phase increased significantly (Fig. 5c), thus confirming the well-accepted idea that strain accumulation decreases microstructure stability and promotes recrystallization. At this stage, the "recrystallized" microstructure was distinctly bimodal consisting of fine (~1 μm) and coarse (~5 μm) grains (Figs. 5c, 6c and 7a). The boundary between the fine and coarse recrystallized grains lay at ~2 μm (Fig. 7a), a value somewhat larger than the critical nucleus size estimated above. The coarse grains were elongated along the RD and contained a high fraction of twins (Fig. 5c). A comparison of the grain-size distributions for the various rolling reductions (Fig. 7a) suggested that the finer grains grew relatively little with additional strain thus indirectly confirming their possibly unstable nature. On the other hand, the volume fraction and size of the coarse grains increased noticeably with increasing reduction (Figs. 5c and 7a).

To rationalize the bimodal nature of the microstructure, the number of "recrystallized" grains per unit area was measured as a function of accumulated strain. The resulting plot (Fig. 7b) revealed that fine grains were continuously nucleated, but very few grew into coarse ones. Thus, it may be hypothesized that the development of the coarse "recrystallized" grains was associated with preferential growth of selected nuclei having an initial size larger than ~1-2 μm.

4.1.2. "Deformed" phase

The "deformed" structure in material rolled to 50-pct. reduction was dominated by grains elongated in the RD (Figs. 5a and 6a). The measured mean grain thickness was very close to theoretical predictions based on the geometry of homogeneous plane-strain compression imposed at the mid-plane during flat rolling (Fig. 8a). A small number of twins was found in the interior of "deformed" grains (Figs. 5a and 6a). This confirms the activation of mechanical twinning during cryogenic deformation of copper [2, 3]. In addition to the twins, the "deformed" grains contained dense sub-boundary networks (Fig. 6a). The subboundaries were typically low-angle in nature; only sporadic HAB segments were seen.

The shape of the LABs in samples rolled to 50-pct. reduction was typically irregular (Fig. 6a). This appearance contrasts with the well-developed, planar dense dislocation walls typically observed in FCC metals of high-to-intermediate stacking fault energy (including copper) deformed at *room* temperature [e.g.18]. The effect may be associated with the suppression of cross-slip at cryogenic temperature [5], thereby hindering dislocation rearrangement into well-developed subboundaries.

After 75-pct. reduction, the mean grain thickness was measurably larger than that based on strictly geometrically considerations (Fig. 8a). In addition, the grain orientation spread in the “deformed” phase was somewhat lower than in material deformed to 50-pct. reduction (Fig. 8b). These observations suggest that the room-temperature annealing process is not merely limited by the development of the “recrystallized” grains but it also involves significant changes in the “deformed” material such as that due to recovery.

A noticeable microstructural feature of the “deformed” phase after 75-pct. reduction was the presence of numerous bulges along the boundaries of the compressed grains; several examples are circled in Fig. 6b. These bulges provided evidence of local grain-boundary migration. Another important feature of the process was the observation that the HABs were frequently curved at triple points with LABs (Fig. 6b). The development of the grain-boundary bulging tended to break up the elongated grains into shorter segments (the region shown by the arrow in Fig. 6b) thus leading to a decrease in the aspect ratio of the deformed grains (Fig. 8c). A similar effect has been observed and analyzed by Prangnell, et al. [19]. It was conclusively demonstrated in this former paper that the annealing behavior of highly deformed material is significantly influenced by substructure. Due to surface tension effects at triple joints including low-mobility LABs, high-mobility HABs cannot migrate uniformly but become noticeably bowed. Such behavior leads to the break-up of elongated, deformed grains into lower-aspect-ratio strings. Hence, although room-temperature annealing of heavily cryo-rolled copper leads to grain-boundary migration in the “deformed” phase, the presence of the dense substructure disrupts uniform grain growth and promotes bulge formation. Some of the bulges transform into recrystallization nuclei whereas others subdivide elongated grains into low-aspect-ratio segments.

After 93-pct. reduction, the measured mean grain thickness was ~5 times larger than the prediction based on the imposed strain (Fig. 8a). The “deformed” microstructure was dominated by relatively low-aspect-ratio grains whereas very long grains had almost completely disappeared (Figs. 5c and 8c). Close inspection of the high-resolution EBSD map (Fig. 6c) revealed numerous evidence of grain growth and grain break-up in the “deformed” phase. All these observations also indicate boundary migration in the “deformed” phase.

The “deformed” phase of the material reduced 93 pct. also showed a significant reduction in the width and magnitude of the grain-orientation spread (Fig. 8b). This result is suggestive of static recovery. At low temperatures, recovery is generally believed to compete with recrystallization, and therefore it is reasonable to expect that it should play a substantial role at room temperature in

the present situation. Recovery may reduce dislocation density (i.e., the driving force for recrystallization) and thus increase the critical (stable) nucleus size from the above prediction of 1 μm to the observed value of 2 μm (Fig. 7a).

After 93-pct. reduction, the LABs in the growing grains tended to become somewhat straighter; several examples are indicated with arrows in Fig. 6c. This effect may be associated with recovery-driven absorption of dislocations by LABs. This would increase the misorientation of the LABs (and thus their mobility); the subboundaries could then lower their energy through local migration.

On the other hand, no signs of gross subgrain growth were observed. Due to the ultrafine-grained nature of the material, the subgrains typically had a mixed LAB/HAB perimeter (Fig. 6) and thus subgrain/grain coarsening occurred via migration of the HAB segments, as discussed above.

4.2. Misorientation distributions

Additional insight into the room-temperature annealing process was obtained from misorientation data extracted for the separated "recrystallized" and "deformed" phases (Figs. 9a and b, respectively). The misorientation-angle data were expressed in terms of the specific grain-boundary length, i.e., the total boundary length in the specific phase divided by the area of that phase in the EBSD map. As shown previously [5, 20], this approach allows a more direct comparison of grain boundary statistics in different phases and simplifies the interpretation of the physical mechanisms governing microstructure evolution.

Because the "recrystallized" grains tended not to impinge on each other (Figs. 5 and 6), the corresponding misorientation-angle distribution (Fig. 9a) essentially reflected (a) surrounding substructure of LABs and (b) Σ3 and Σ9 annealing-twin boundaries producing peaks near 60° and 40°, respectively. As shown in the figure, substructure of LABs dominated after 50 pct. reduction. With increasing strain, however, the specific boundary length associated with LABs decreased significantly, probably indicating that the LABs in the "recrystallized" phase gradually annealed out. By contrast, annealing twins became more dominant with increasing prior deformation; i.e., the Σ3 boundary fraction was ~30 pct. in material reduced in thickness by 93 pct.

In the "deformed" phase, the low-angle portion of the misorientation distribution (Fig. 9b) also exhibited significant changes with increasing strain. The specific length of the very low-angle (2-3°) boundaries decreased noticeably. These boundaries were most likely consumed by local boundary migration in the "deformed" phase. On the other hand, the specific length of highly-misoriented LABs (~10-15°) grew with rolling reduction. This effect may be associated with static recovery, as discussed in the Section 4.1.2.

Because the misorientation data were obtained from the longitudinal (the RD-ND) section, the HAB area in the "deformed" phase should increase with strain due to the geometrical compression of grains during rolling. Indeed, this effect was seen in the range of 50–75 pct. reduction (Fig. 9b). After 93 pct reduction, however, the specific length of HABs changed only slightly, thus mirroring the very small reduction in grain thickness (Fig. 8a).

4.3. Texture

Orientation data in terms ODFs (Fig. 10) and individual texture components (Fig. 11) as a function of rolling reduction provided further insight into the nature of the "deformed" and "recrystallized" regions.

The texture in the "deformed" phase (Figs. 10 and 11a) was mainly composed of the Brass {011}<211> and S_3 {123}<634> components. Previously, the preferential development of the Brass texture (instead of the copper {112}<111> component) was attributed to the suppression of the cross-slip at cryogenic temperature, whereas the large proportion of the S_3 component was associated with the remnants of the β fiber formed at low rolling reductions [5].

In the "recrystallized" phase, the preferential grain orientations after 50 and 75 pct. rolling reductions were generally close to the respective deformation textures (Figs. 10 and 11b). This observation indicates that the recrystallization nuclei originating from local grain-boundary bulging inherited the crystallographic orientation of the deformed grains. This is as expected for discontinuous recrystallization governed by local grain-boundary migration [17].

After 93 pct of rolling, however, the texture patterns in the "deformed" and "recrystallized" phases were distinctly different (Fig. 10). The observed significant strengthening of the Taylor component {4;4;11}<11;11;8> (Fig. 11b) is of particular interest. An EBSD texture-component map (Fig. 12) indicated that the Taylor (as well as Copper) components were mainly produced by the coarse "recrystallized" grains. It is worth noting in this regard, that the Taylor and Copper orientations are characterized by the highest number of active slip systems (five and four, respectively) operating during rolling [21]. A large number of active slip systems is known to promote the formation of well-defined dislocation boundaries thus decreasing the density of free dislocations. Hence, the Taylor and Copper orientations may have lower stored energy than the other rolling components and thus would be expected to have an advantage in forming nuclei via *recovery* which may then undergo growth into the deformed matrix. This suggests that the coarse "recrystallized" grains observed in the heavily rolled material (Figs. 5c, 6c and 7a) originated as a result of recovery rather than grain-boundary bulging. Indeed, it is unlikely that the stable (>2 μm) recrystallization nuclei originated from the fine-scale grain-boundary bulges in submicrocrystalline "deformed" grains (Figs. 6 and 8a). It seems more probable that the "deformed" grains first coarsened and recovered thus gradually transforming into stable "recrystallized" grains. The bimodal nature of the "recrystallized" structure in material rolled to 93-pct. reduction (Fig. 7a) appears to support the occurrence of competing nucleation mechanisms.

5. SUMMARY AND CONCLUSIONS

The EBSD technique was applied to investigate the room-temperature annealing behavior of cryogenically-rolled copper during long-term (~1.5 years) static storage. It was found that the room-temperature annealing processes include grain-boundary migration (accompanied by annealing twinning) and recovery. Due to the pinning effect associated with low-mobility LABs, grain-boundary migration degenerates into local boundary bulging which breaks up

elongated grains into lower-aspect ratio segments and gives rise to very fine (<2 μm) recrystallization nuclei. Because of the very fine size of these nuclei, they are unable to grow and thus unlikely to affect the global recrystallization behavior. On the other hand, the simultaneous occurrence of recovery in the deformed matrix was shown to reduce orientation spread and promote LAB development, thus gradually transforming the selected deformed grains into stable (~5 μm) recrystallization nuclei. The competition between two nucleation mechanisms produces a bimodal recrystallized structure. Grains with particular crystallographic orientations (e.g., Taylor or Copper) appear to have an advantage in the recovery process. This effect was attributed to the high number of active slip systems operating during rolling which promotes the formation of well-developed dislocation boundaries and thus reduced stored energy associated with free dislocations.

Acknowledgments

The authors gratefully acknowledge Professor G.A. Salishchev and Dr. M.A. Murzinova for suggesting this research. They also thank Dr. R.M. Galeyev and Dr. O.R. Valiakhmetov for graciously providing the material used in this work and Dr. R.R. Daminov for technical assistance.

References

[1] Y. Huang, P.B. Prangnell, The effect of cryogenic temperature and change in deformation mode on the limiting grain size in a severely deformed dilute aluminium alloy, Acta Mater. 56 (2008) 1619–1632.
[2] Y.S. Li, N.R. Tao, K. Lu, Microstructural evolution and nanostructure formation in copper during dynamic plastic deformation at cryogenic temperatures, Acta Mater. 56 (2008) 230–241.
[3] Y. Zhang, N.R. Tao, K. Lu, Mechanical properties and rolling behaviors of nano-grained copper with embedded nano-twin bundles, Acta Mater. 56 (2008) 2429–2440.
[4] Y. Estrin, N.V. Isaev, S.V. Lubenets, S.V. Malykhin, A.T. Pugachov, V.V. Pustovalov, E.N. Reshetnyak, V.S. Fomenko, L.S. Fomenko, S.E. Shumilin, M. Janecek, R.J. Hellmig, Effect of microstructure on plastic deformation of Cu at low homologous temperatures, Acta Mater. 54 (2006) 5581–5590.
[5] T. Konkova, S. Mironov, A. Korznikov, S.L. Semiatin, Structural response of pure copper to cryogenic rolling, Acta Materialia 58 (2010) 5262-5273.
[6] H.D. Meingelberg, M. Meixner, K. Lucke, The kinetics of the recrystallization of copper deformed at low temperatures, Acta Metal. 13 (1965) 835-844.
[7] J. Tarasiuk, Ph. Gerber, B. Bacroix, Estimation of recrystallized volume fraction from EBSD data, Acta Mater. 50 (2002) 1467-1477
[8] D.P. Field, L.T. Bradford, M.M. Nowell, T.M. Lillo, The role of annealing twins during recrystallization of Cu, Acta Mater. 55 (2007) 4233-4241.
[9] G. Wu, D.Juul Jensen, Automatic determination of recrystallization parameters based on EBSD mapping, Mater. Character. 59 (2008) 794-800.
[10] S. Dziaszyk, E.J. Payton, F. Friedel, V. Marx, G. Eggeler, On the characterization of recrystallized fraction using electron backscatter diffraction: a direct comparison to local hardness in an IF steel using nanoindentation, Mater. Sci. Eng. A527 (2010) 7854-7864.
[11] F.J. Humphreys, Quantitative metallography by electron backscatter diffraction, J. Microscopy 195 (1999) 170-185.
[12] D.P. Field, Recent advances in the application of orientation imaging, Ultramicroscopy 67 (1997) 1-9.
[13] T.J. Sabin, G. Winther, D. Juul Jensen, Orientation relationship between recrystallization nuclei at triple junctions and deformed structures, Acta Mater. 51 (2003) 3999-4011.

[14] D.T. McDonald, F.J. Humphreys, P.S. Bate, Microstructure and texture of dynamically recrystallized copper and copper-tin alloys, Mater. Sci. Forum 550 (2007) 393-398.
[15] Ye.V. Nesterova, V.V. Rybin, Mechanical twinning and the fragmentation of commercial titanium at the stage of developed plastic deformation, Phys. Met. Metall. 59 (1985) 169-179.
[16] D. Dingley, Progressive steps in the development of electron backscatter diffraction and orientation imaging microscopy, J. Microscopy 213 (2004) 214-224.
[17] F.J. Humphreys, M. Hatherly, Recrystallization and related phenomena, Elsevier, 2004, 574p.
[18] N. Hansen and D. Juul Jensen, Development of microstructure in FCC metals during cold work, Phil. Trans. R. Soc. Lond. A 357 (1999) 1447-1469.
[19] P.B. Prangnell, J.S. Hayes, J.R. Bowen, P.J. Apps, P.S. Bate, Continuous recrystallization of lamellar deformation structures produced by severe deformation, Acta Mater. 52 (2004) 3193-3206.
[20] T. Konkova, S. Mironov, A. Korznikov, S.L. Semiatin, Microstructure instability of cryogenically-deformed copper, *Scripta Materialia*, 63 (2010) 921-924.
[21] J. Hirsch and K. Lucke, Mechanism of deformation and development of rolling textures in polycrystalline F.C.C. metals – II. Simulation and interpretation of experiments on the basis of Taylor-type theories, Acta Metall. 36 (1988) 2883-2904.

Table 1. Ideal rolling and recrystallization textures for face-centered cubic metals

Orientation	Euler angles, deg			Miller indices	
	φ_1	Φ	φ_2	Normal direction	Rolling direction
Rolling textures					
Cube	0	0	0	{001}	<100>
Goss	0	45	90	{011}	<100>
Brass	35	29	63	{011}	<211>
S_3	59	37	63	{123}	<634>
Copper	90	35	45	{112}	<111>
Taylor	90	27	45	{4;4;11}	<11;11;8>
Recrystallization textures					
Cube	0	0	0	{001}	<100>
Goss	0	45	90	{011}	<100>
P	70	45	0	{011}	<122>
Q	58	18	0	{013}	<231>

Figure Captions

Figure 1. EBSD maps used to partition the deformed/recrystallized regions in copper cryogenically rolled to a 93-pct. thickness reduction: (a) Image quality, (b) confidence index, (c) grain-orientation-spread, and (d) grain-orientation-spread map with superimposed grain boundaries. In (c) and (d), grains with an orientation spread lower or higher than 2° are colored white and gray, respectively. In (d), LABs, HABs, and Σ3 boundaries (within a 5° tolerance) are depicted by green, black, and red lines, respectively.

Figure 2. Frequency distributions of (a) image quality and (b) confidence index for grains with an orientation spread below and above 2°.

Figure 3. (a) Misorientation-angle distributions and (b) deviations of the twin-boundary misorientation from the ideal Σ3 for grains with an orientation spread below and above 2°.

Figure 4. Orientation distribution functions for material with a grain orientation spread (a) above and (b) below 2°.

Figure 5. Low-resolution grain-orientation-spread maps for copper cryogenically rolled to a thickness reduction of (a) 50 pct. (b) 75 pct., or (c) 93 pct. The “recrystallized” and “deformed” grains are colored white and gray, respectively. HABs and Σ3 boundaries (within a 5° tolerance) are depicted by black and red lines, respectively.

Figure 6. High-resolution grain-orientation-spread maps for copper cryogenically rolled to a thickness reduction of (a) 50 pct., (b) 75 pct., or (c) 93 pct. The “recrystallized” and “deformed” grains are colored white and gray, respectively. HABs and Σ3 boundaries (within a 5° tolerance) are depicted by black and red lines, respectively.

Figure 7. Effect of rolling reduction on (a) grain size in “recrystallized” material and (b) number of “recrystallized” grains per unit area. The twin boundaries were ignored in both cases.

Figure 8. Effect of rolling reduction on grain-structure characteristics in “deformed” material: (a) mean grain thickness, (b) grain orientation spread, and (c) grain-shape aspect ratio. The error bars in (a) indicate the standard deviation in the measurements.

Figure 9. Effect of rolling reduction on the misorientation-angle distribution in (a) “recrystallized” and (b) “deformed” regions.

Figure 10. Effect of rolling reduction on the texture in the “deformed” and “recrystallized” regions.

Figure 11. Effect of rolling reduction on the volume fractions of the observed texture components (within 10° of the ideal orientations) in (a) “deformed” and (b) “recrystallized” regions.

Figure 12. Spatial distribution of the main texture components (within 10° of the ideal orientations) in material reduced 93-pct. in thickness.

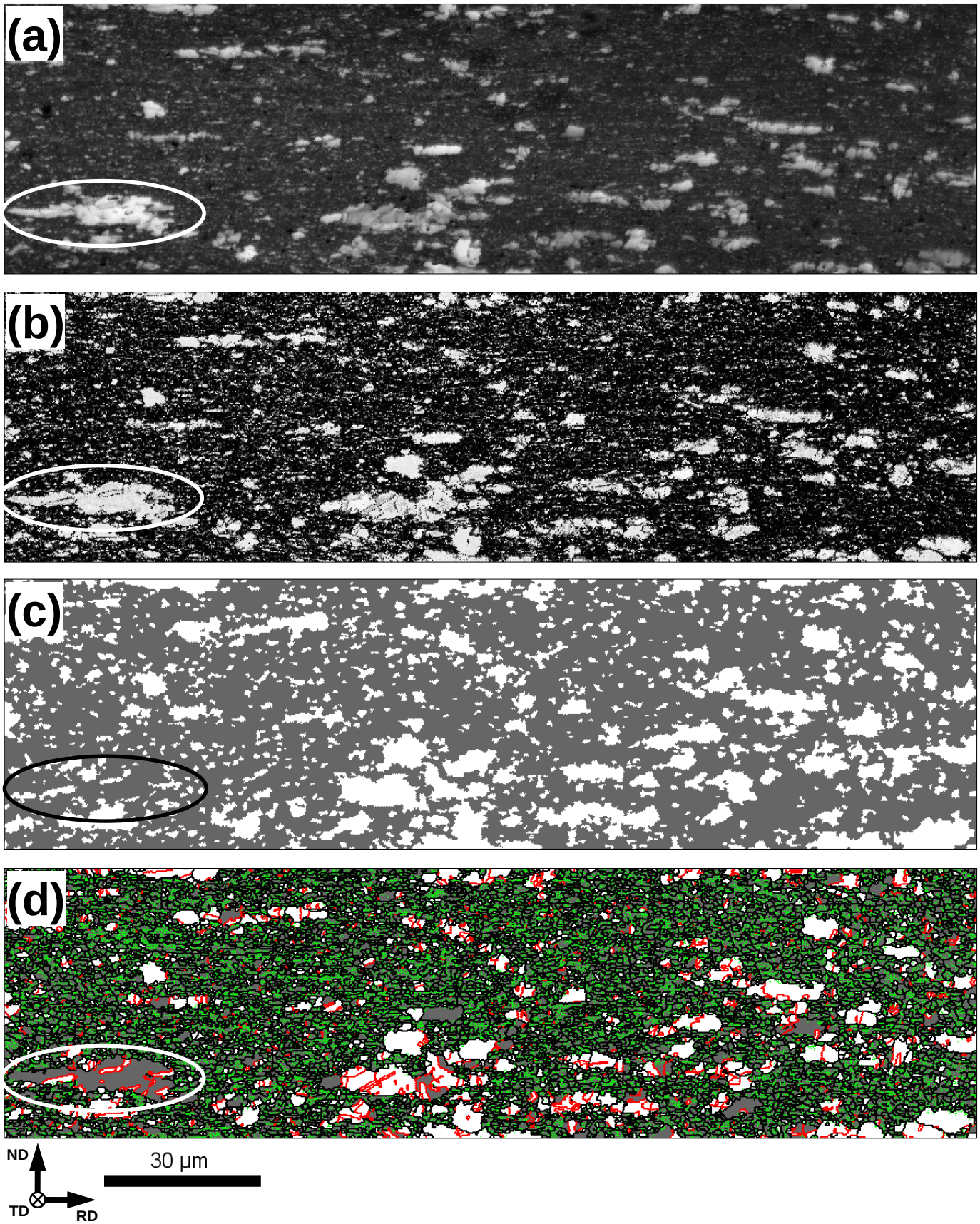

Figure 1. EBSD maps used to partition the deformed/recrystallized regions in copper cryogenically rolled to a 93-pct. thickness reduction: (a) Image quality, (b) confidence index, (c) grain-orientation-spread, and (d) grain-orientation-spread map with superimposed grain boundaries. In (c) and (d), grains with an orientation spread lower or higher than 2° are colored white and gray, respectively. In (d), LABs, HABs, and Σ3 boundaries (within a 5° tolerance) are depicted by green, black, and red lines, respectively.

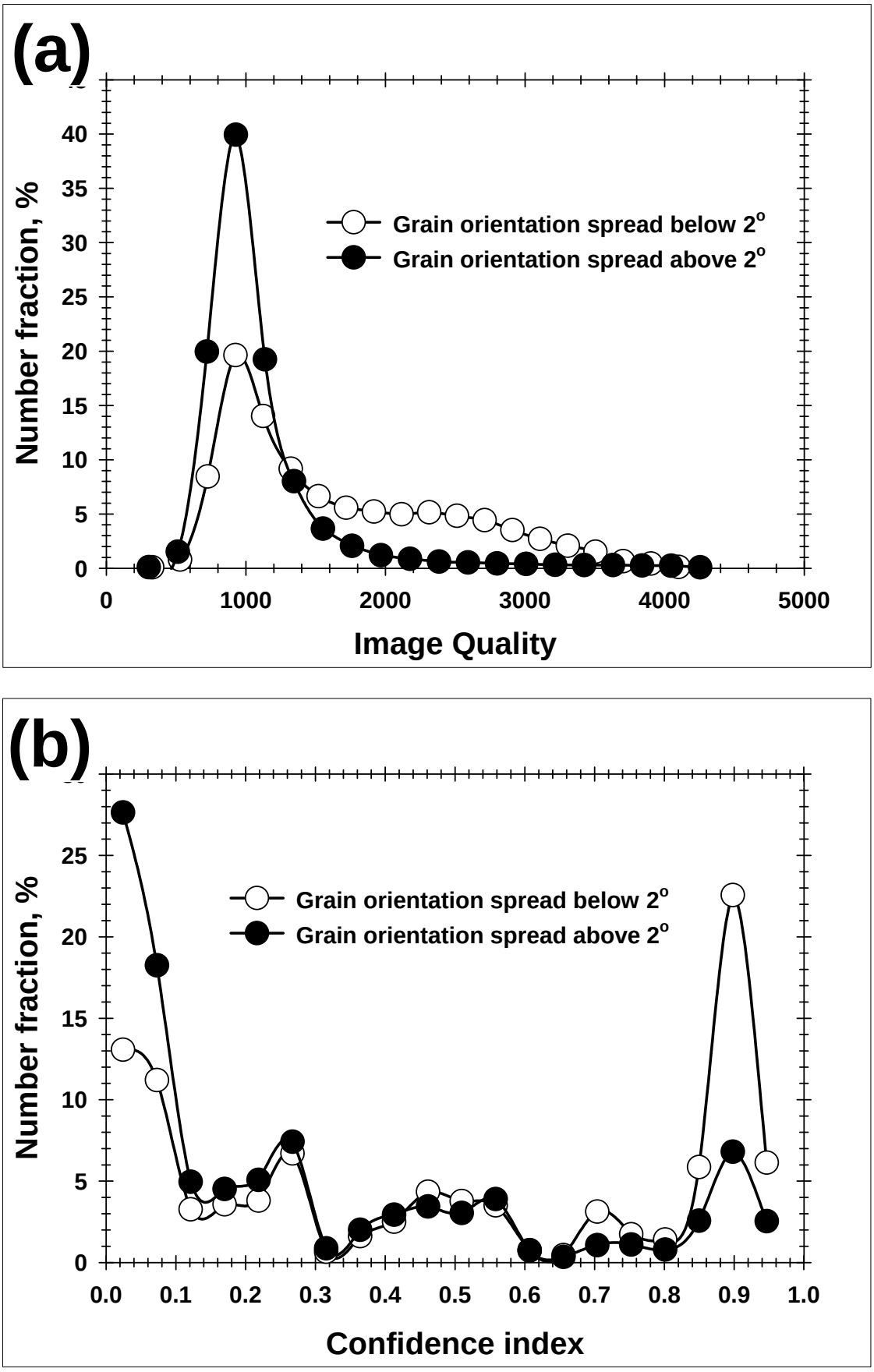

Figure 2. Frequency distributions of (a) image quality and (b) confidence index for grains with an orientation spread below and above 2°.

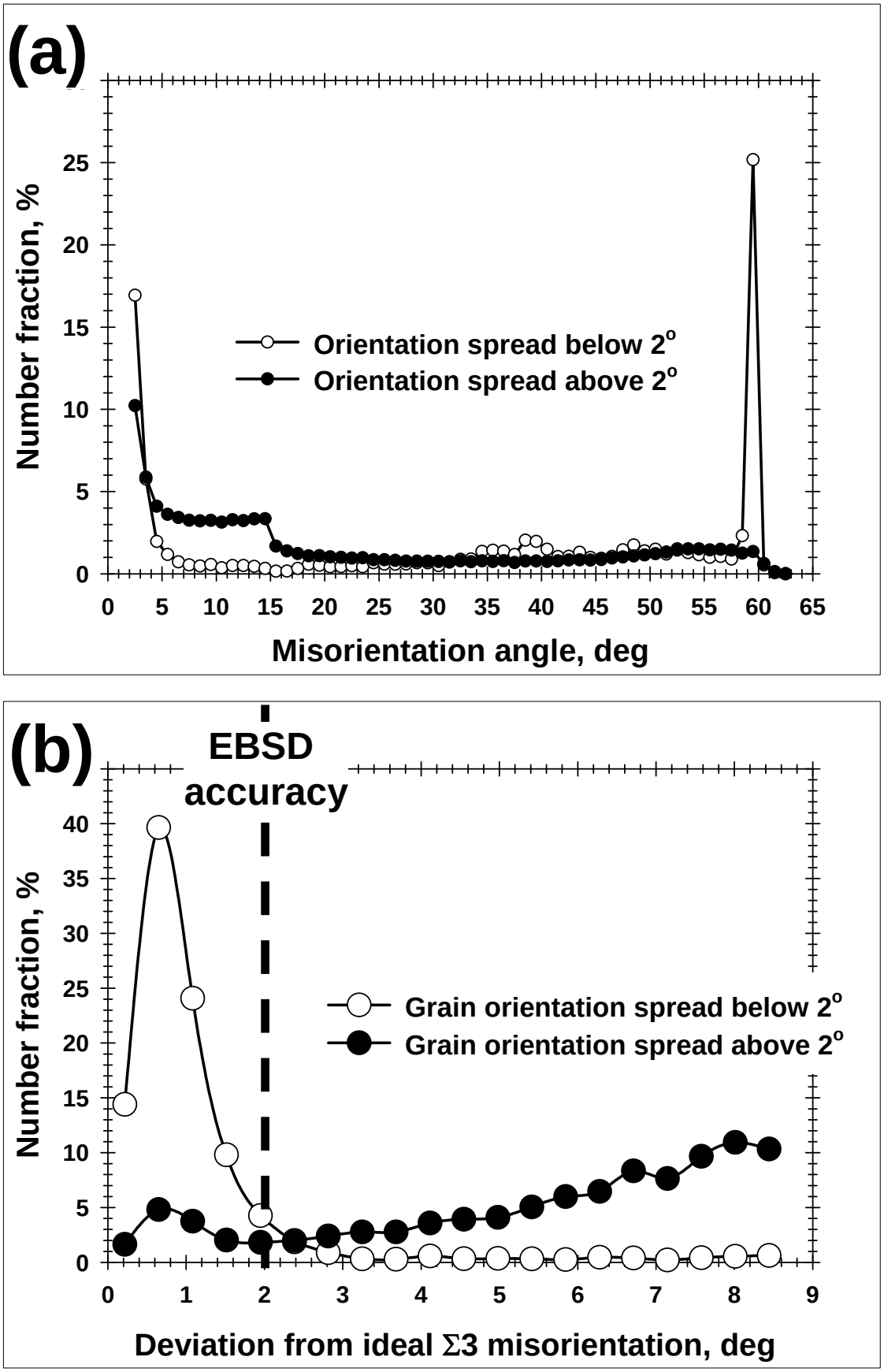

Figure 3. (a) Misorientation-angle distributions and (b) deviations of the twin-boundary misorientation from the ideal Σ3 for grains with an orientation spread below and above 2°.

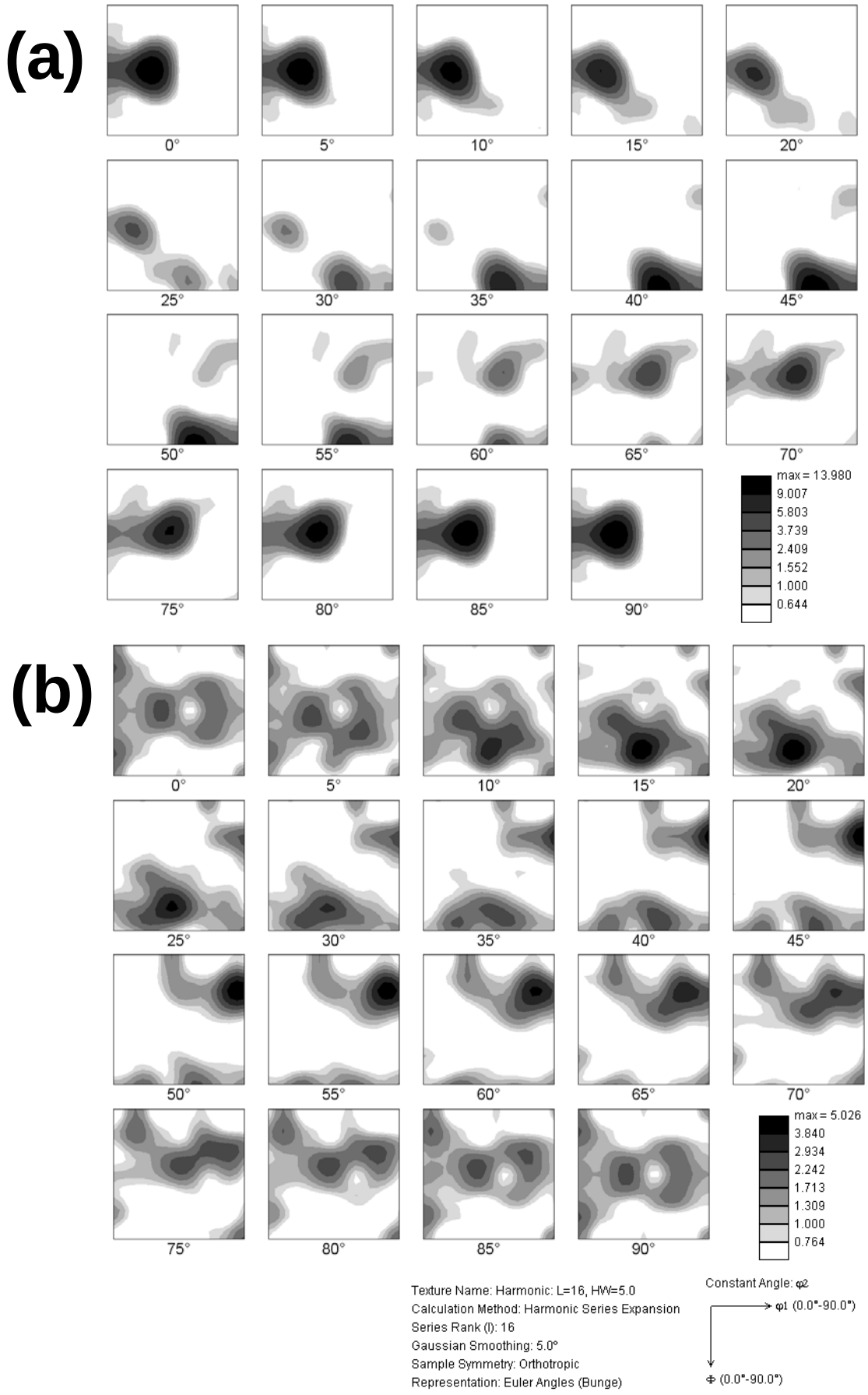

Figure 4. Orientation distribution functions for material with a grain orientation spread (a) above and (b) below 2°.

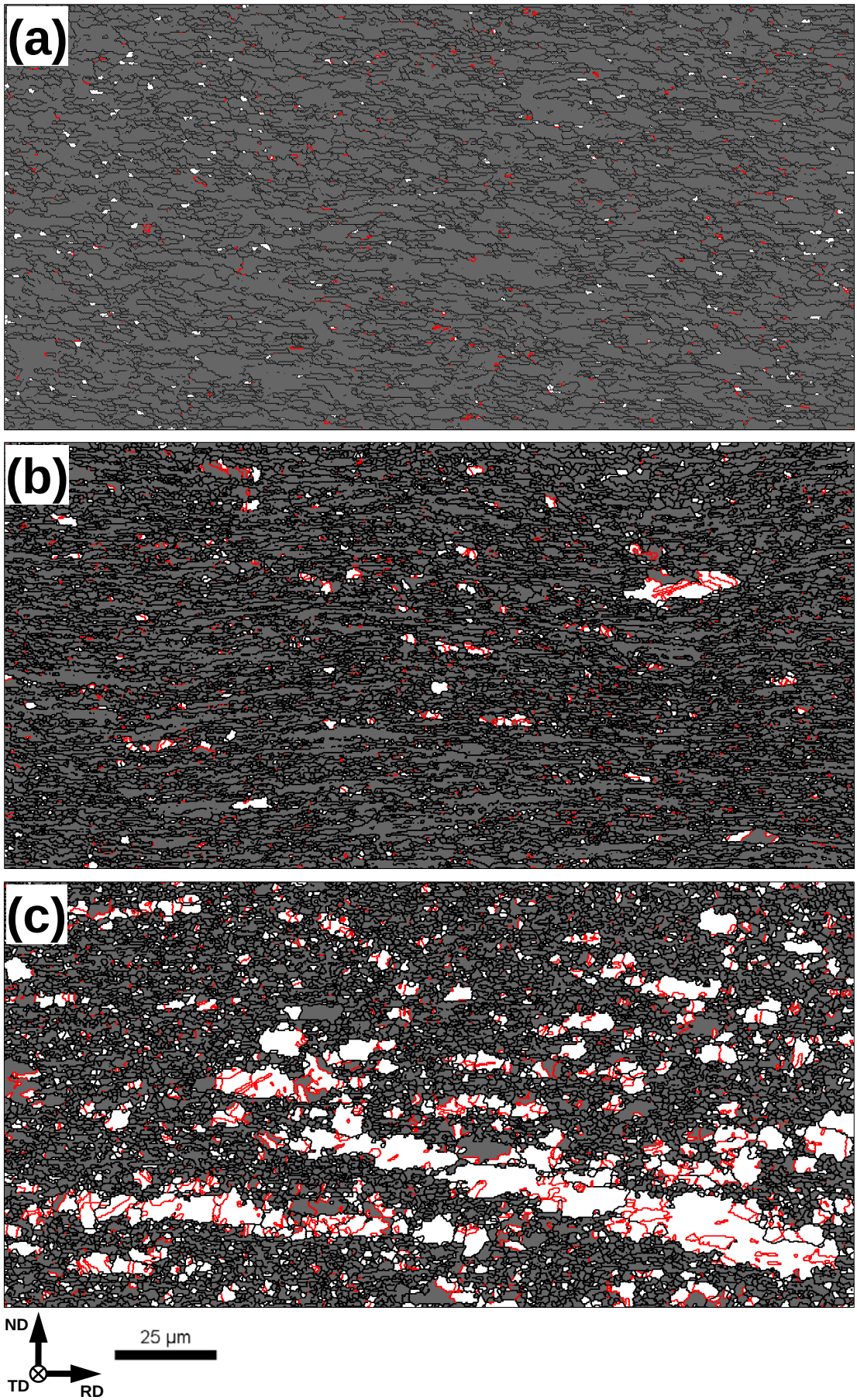

Figure 5. Low-resolution grain-orientation-spread maps for copper cryogenically rolled to a thickness reduction of (a) 50 pct. (b) 75 pct., or (c) 93 pct. The “recrystallized” and “deformed” grains are colored white and gray, respectively. HABs and Σ3 boundaries (within a 5° tolerance) are depicted by black and red lines, respectively.

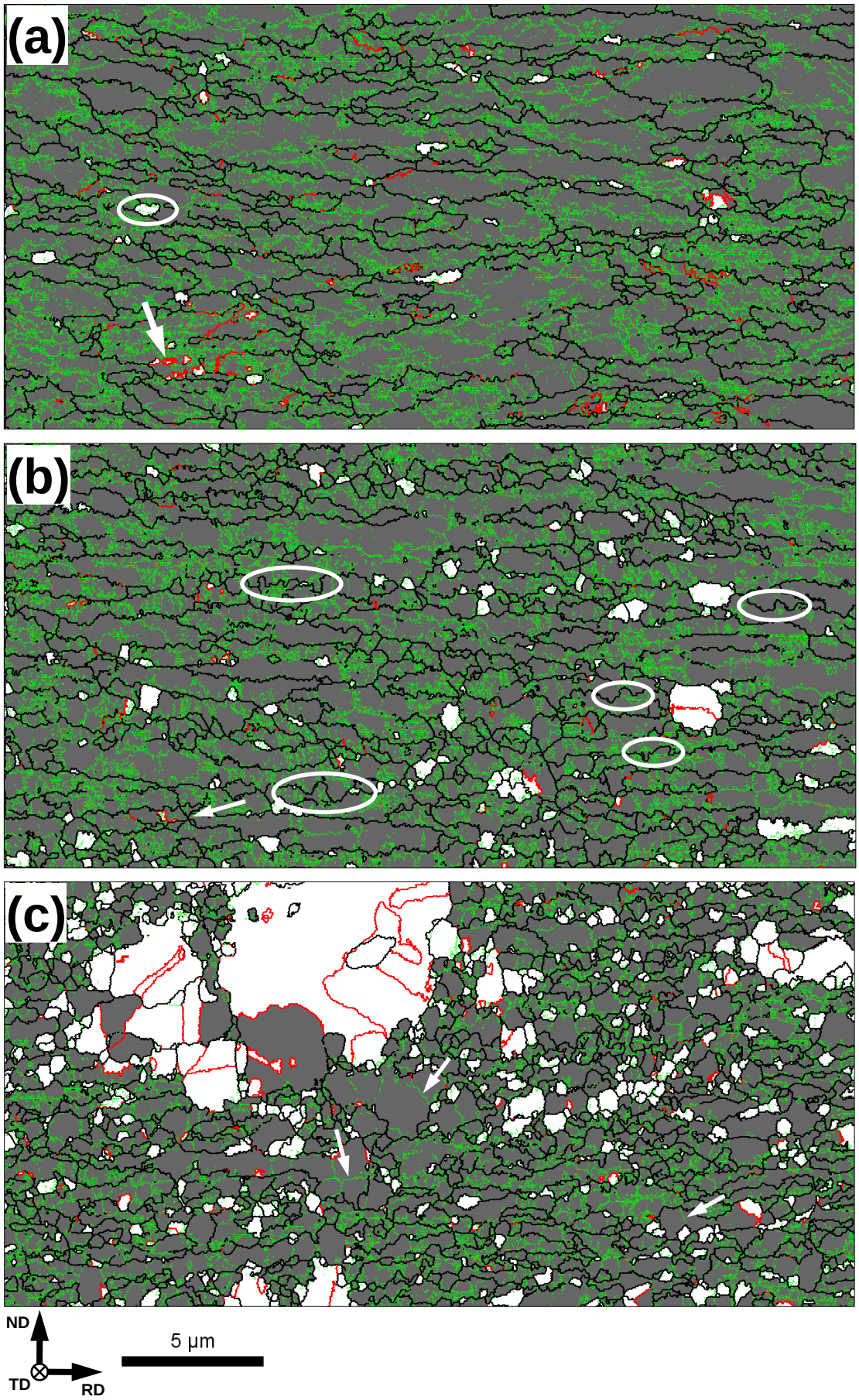

Figure 6. High-resolution grain-orientation-spread maps for copper cryogenically rolled to a thickness reduction of (a) 50 pct., (b) 75 pct., or (c) 93 pct. The “recrystallized” and “deformed” grains are colored white and gray, respectively. HABs and Σ3 boundaries (within a 5° tolerance) are depicted by black and red lines, respectively.

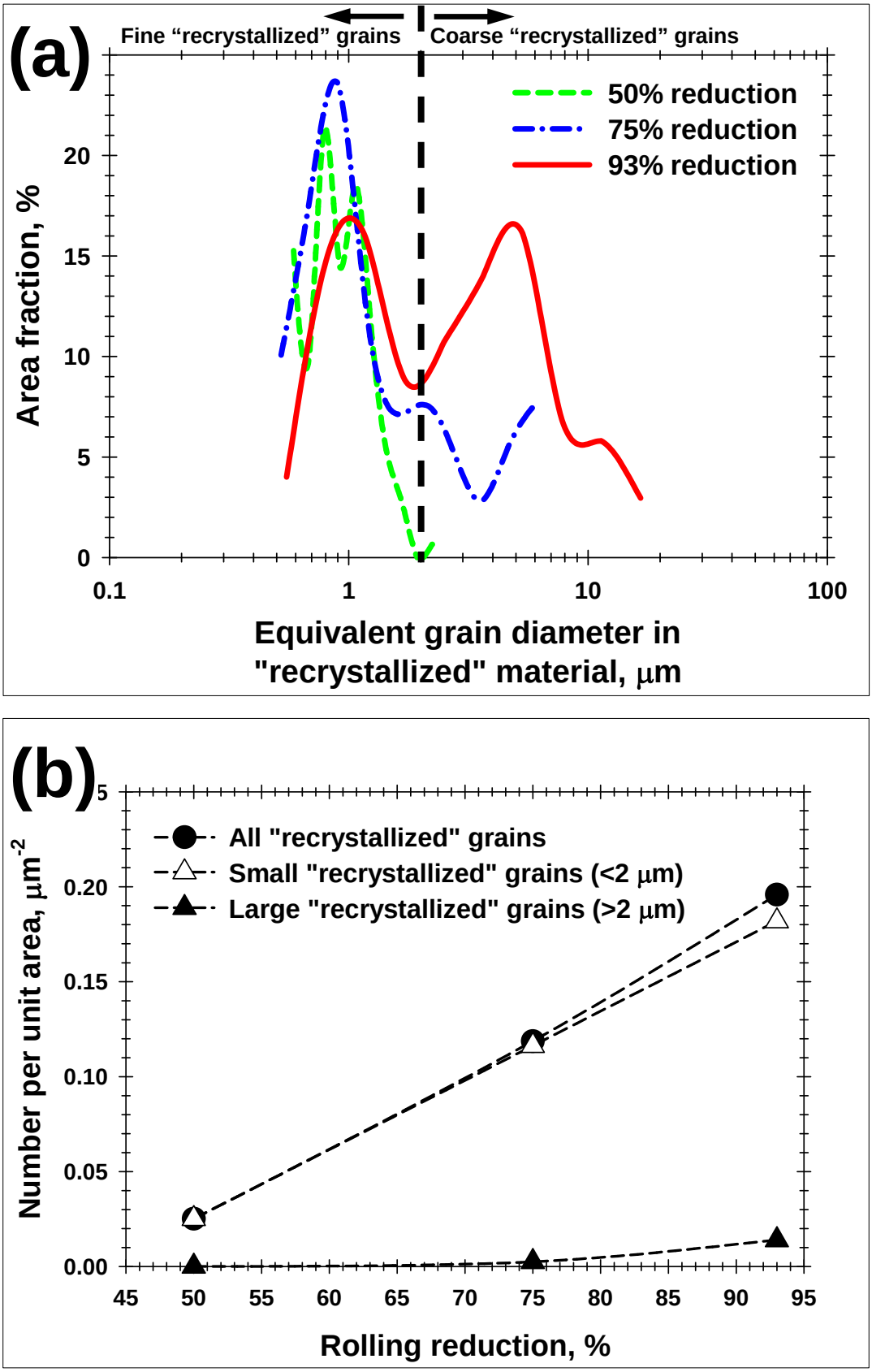

Figure 7. Effect of rolling reduction on grain size in "recrystallized" material (a) and number of the "recrystallized" grains per unit area (b). The twin boundaries were ignored in both cases.

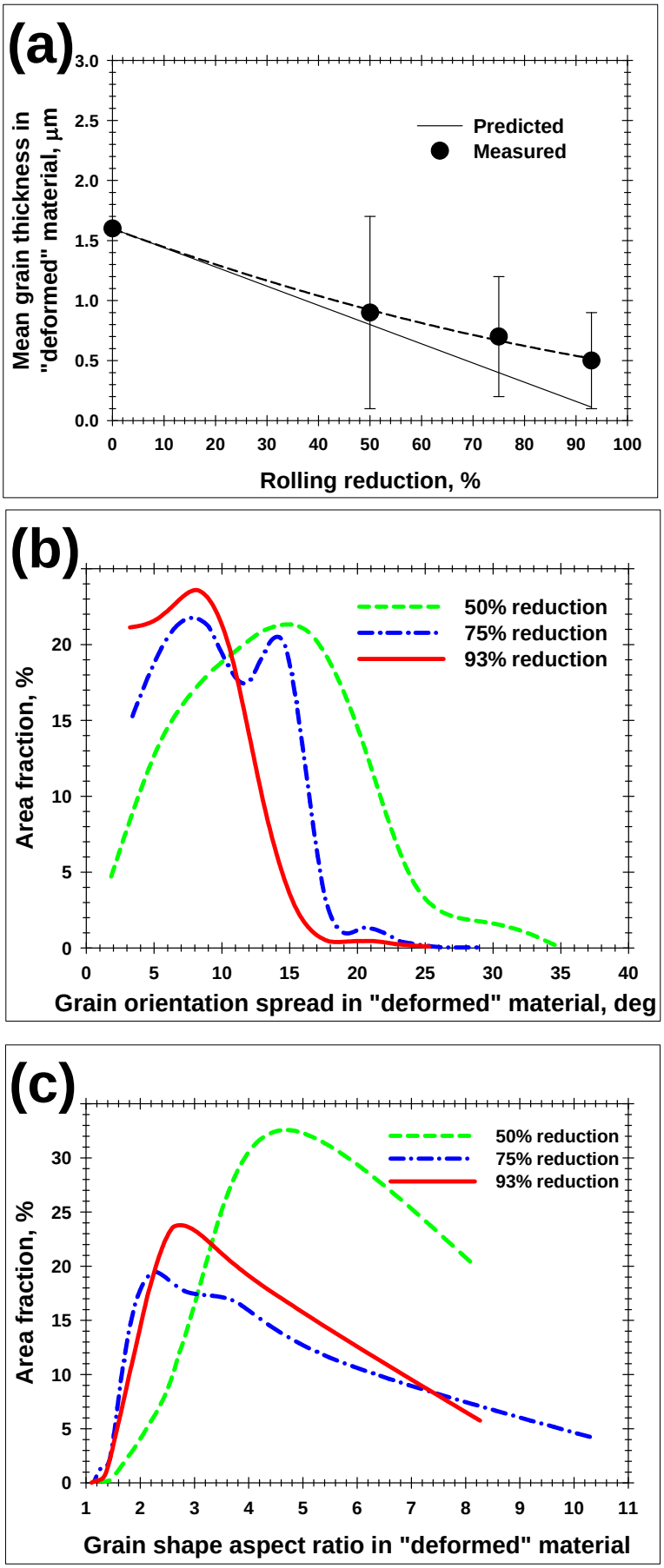

Figure 8. Effect of rolling reduction on grain-structure characteristics in “deformed” material: (a) mean grain thickness, (b) grain orientation spread, and (c) grain-shape aspect ratio, and. The error bars in (a) indicate the standard deviation in the measurements.

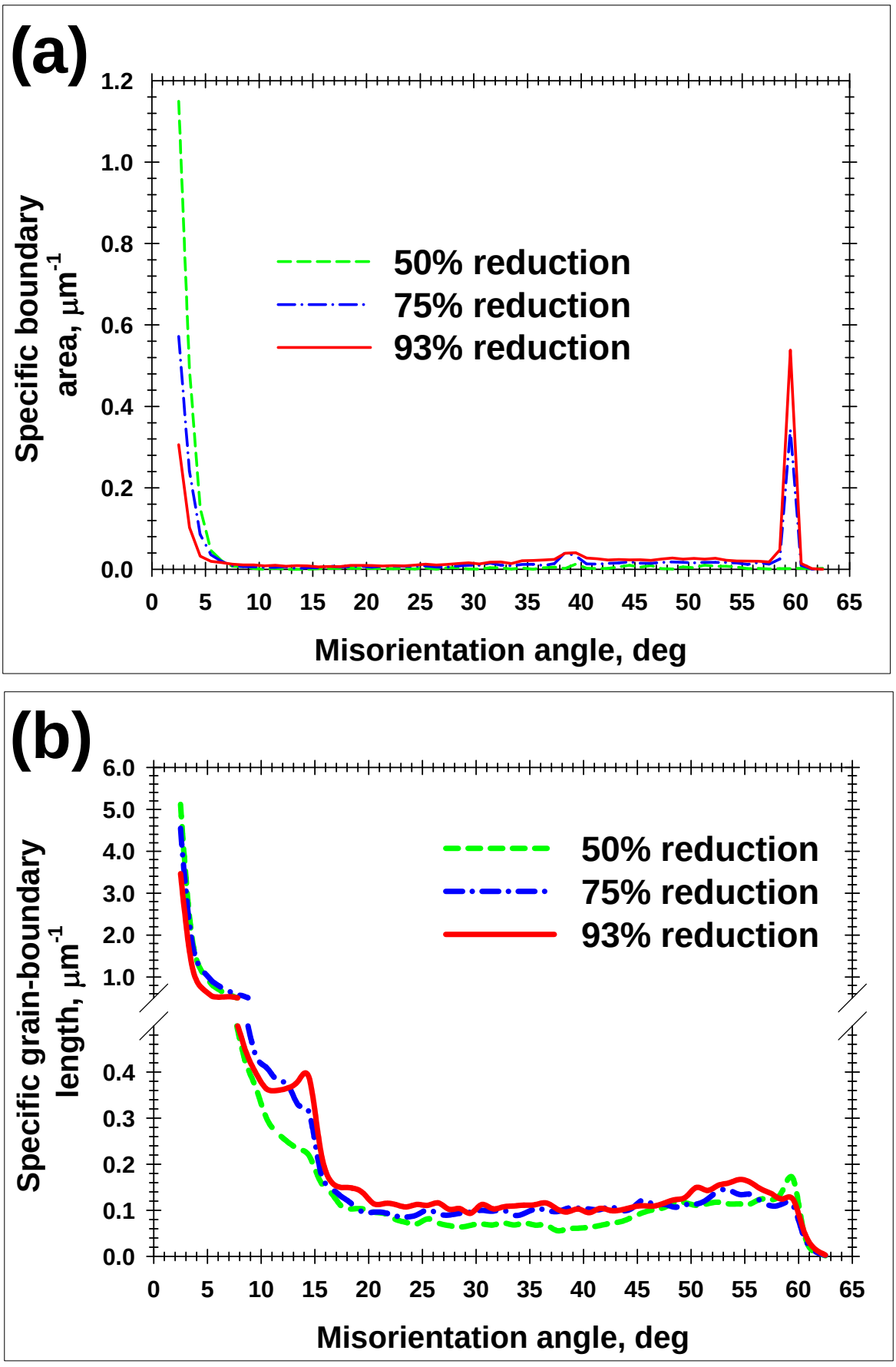

Figure 9. Effect of rolling reduction on the misorientation-angle distribution in (a) “recrystallized” and (b) “deformed” regions.

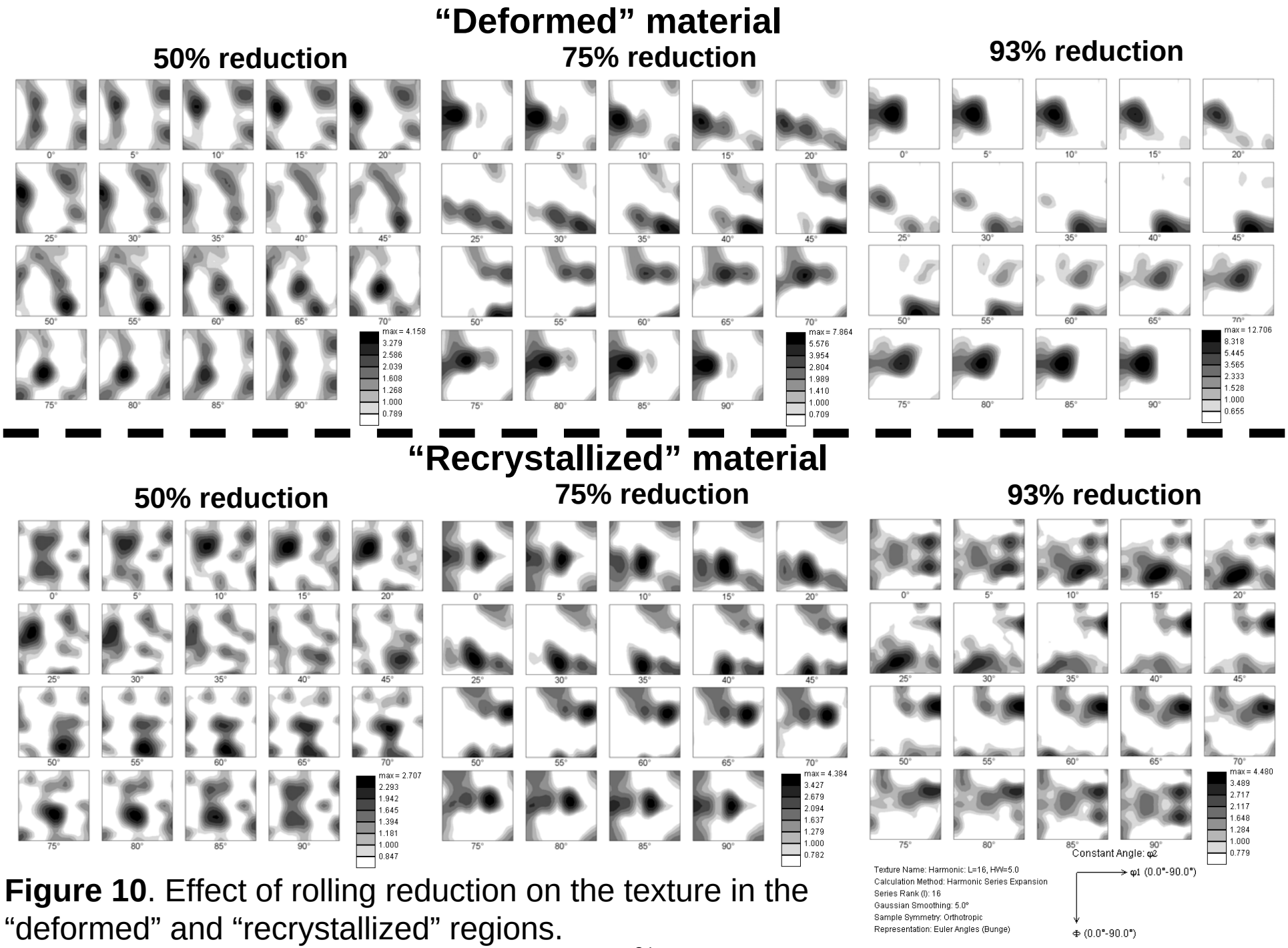

Figure 10. Effect of rolling reduction on the texture in the "deformed" and "recrystallized" regions.

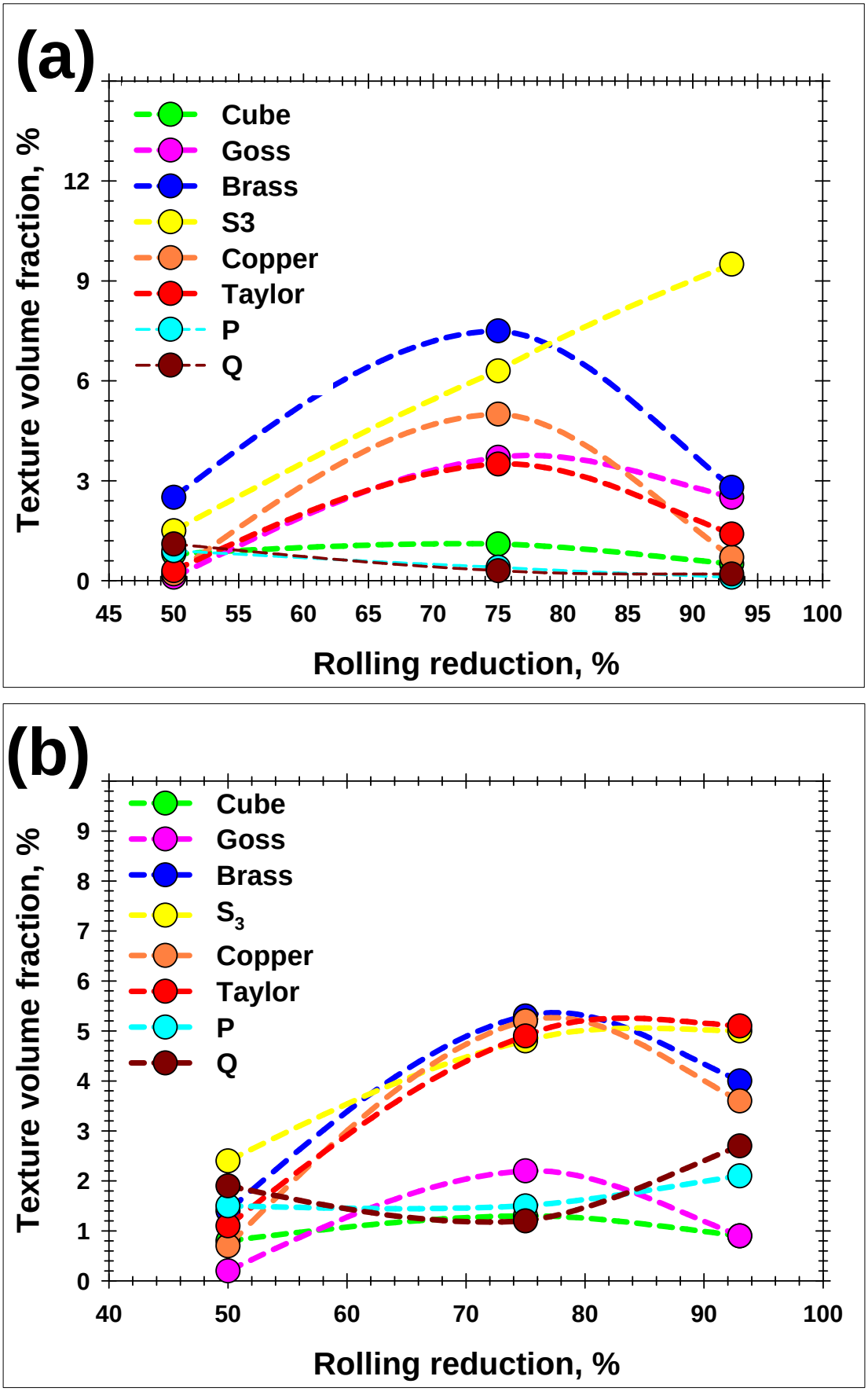

Figure 11. Effect of rolling reduction on the volume fractions of the observed texture components (within 10° of the ideal orientations) in (a) “deformed” and (b) “recrystallized” regions.

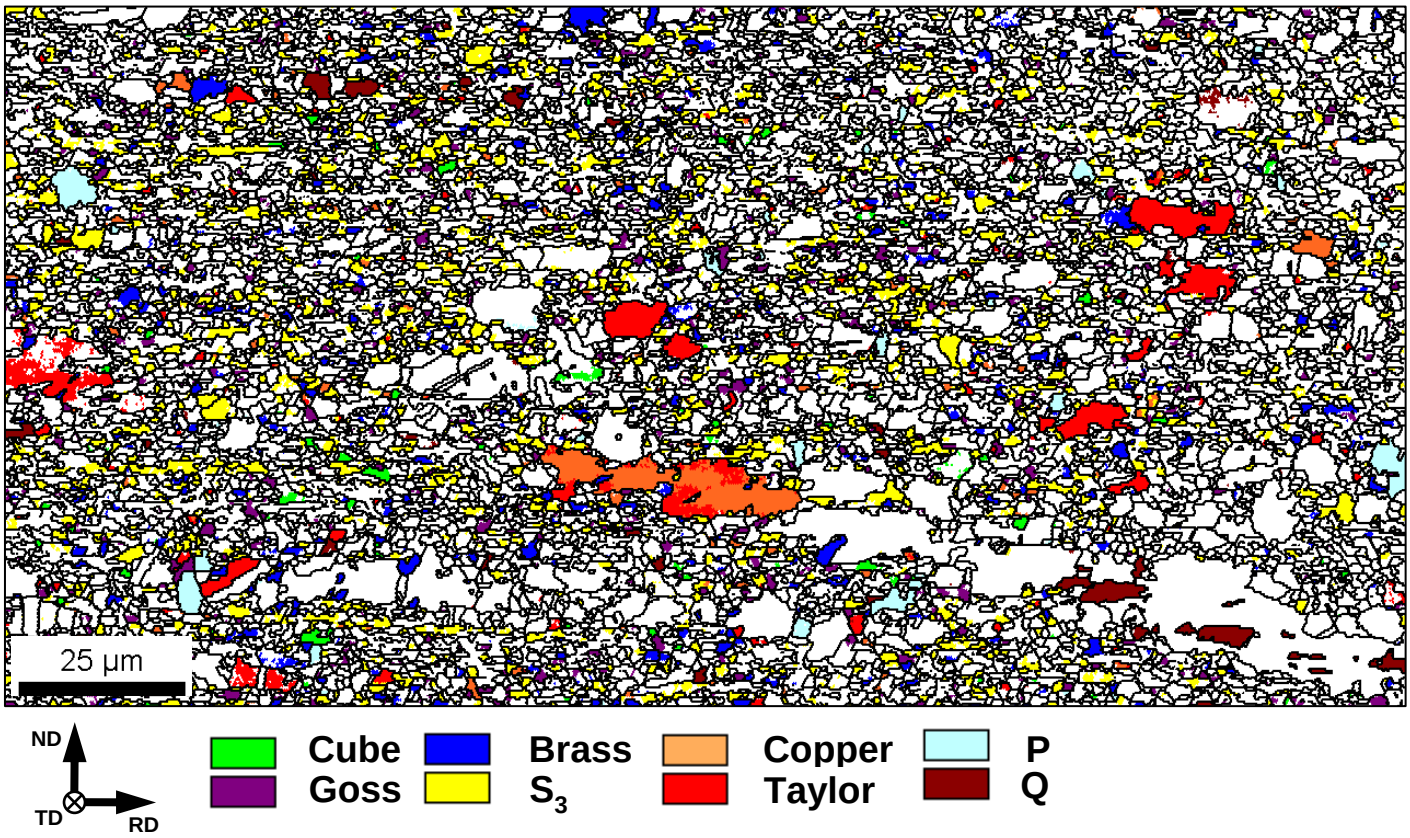

Figure 12. Spatial distribution of the main texture components (within 10° of the ideal orientations) in material reduced 93-pct. in thickness.